Multiwalled Nanotubes Formed by Catanionic Mixtures of Drug Amphiphiles

Yi-An Lin,[†,‡] Andrew G. Cheetham,[†,‡] Pengcheng Zhang,[†,‡] Yu-Chuan Ou,[†] Yuguo Li,[∥] Guanshu Liu,[∥] Daniel Hermida-Merino,[#] Ian W. Hamley,[⊗] and Honggang Cui[*,†,‡,§,⊥]

[†]Department of Chemical & Bimolecular Engineering and [‡]Institute for NanoBiotechnology, Johns Hopkins University, 3400 North Charles Street, Baltimore, Maryland 21218, United States, [§]Department of Oncology and Sidney Kimmel Comprehensive Cancer Center, Johns Hopkins University School of Medicine, Baltimore, Maryland 21205, United States, [⊥]Center for Nanomedicine, The Wilmer Eye Institute, Johns Hopkins University School of Medicine, 400 North Broadway, Baltimore, Maryland 21231, United States, [∥]F. M. Kirby Center, Kennedy Krieger Institute, and Department of Radiology, Johns Hopkins School of Medicine, 707 North Broadway, Baltimore, Maryland 21205, United States, [#]DUBBLE-Dutch Belgian Beamline (BM26), ESRF, 6 Rue Jules Horowitz, BP 220, 38043 Grenoble CEDEX 9, France, and [⊗]Department of Chemistry, University of Reading, Whiteknights, Reading, Berkshire RG6 6UR, United Kingdom

ABSTRACT Mixing of oppositely charged amphiphilic molecules (catanionic mixing) offers an attractive strategy to produce morphologies different from those formed by individual molecules. We report here on the use of catanionic mixing of anticancer drug amphiphiles to construct multiwalled nanotubes containing a fixed and high drug loading. We found that the molecular mixing ratio, the solvent composition, the overall drug concentrations, as well as the molecular design of the studied amphiphiles are all important experimental parameters contributing to the tubular morphology. We believe these results demonstrate the remarkable potential that anticancer drugs could offer to self-assemble into discrete nanostructures and also provide important insight into the formation mechanism of nanotubes by catanionic mixtures. Our preliminary animal studies reveal that the CPT nanotubes show significantly prolonged retention time in the tumor site after intratumoral injection.

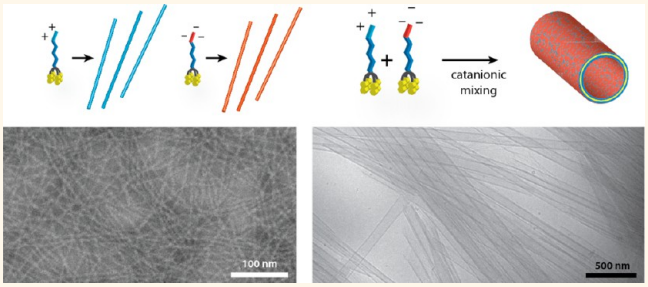

KEYWORDS: self-assembly · nanotubes · catanionic mixtures · drug · camptothecin

Nanotubes are one-dimensional (1D) hollow nanostructures that could possess dimensionality-related electronic,[1] mechanical,[2,3] or biological properties[4,5] and have attracted extensive research interest over the past two decades due to their potential applications in electronics,[6−9] catalysis,[10] and drug delivery.[11,12] From the manufacturing perspective, nanotubes can be produced *via* vapor deposition techniques (*e.g.*, carbon nanotubes,[2] diphenylalanine nanotubes[7]) by using high-aspect-ratio nanostructures as precursors or templates[13] or through solution-state molecular self-assembly,[14,15] a facile process that typically neither requires high temperature nor low pressure and does not involve deposition and etching procedures. A number of molecular building units have been shown capable of spontaneously associating into tubular morphologies upon dissolution into a selective solvent, including block copolymers,[16,17] lipids,[18−21] cholesterol derivatives,[22] peptides,[23−27] and other amphiphilic molecules.[28−30] Of many molecular features appearing to contribute to the formation of tubular assemblies typically composed of bilayer structures, the ability to pack anisotropically in a highly ordered fashion within two dimensions seems to be a general requirement for most molecular building blocks.[15] In this work, we report the first use of anticancer drugs as molecular building blocks to construct a multiwalled nanotube morphology.

Self-assembly of therapeutic agents into well-defined nanoscale objects offers an innovative strategy to construct self-delivering supramolecular nanomedicine with controlled pharmacokinetic properties.[31−37] Since a majority of anticancer drugs do not carry the amphiphilic feature necessary for

* Address correspondence to hcui6@jhu.edu.

Received for review October 6, 2014 and accepted November 21, 2014.

Published online November 21, 2014
10.1021/nn505688b

self-assembling into discrete nanostructures in aqueous environments, an important step in this strategy is the design and construction of amphiphilic drug molecules through conjugation with another hydrophilic chemical moiety.[31−39] The resultant amphiphilic conjugates could potentially serve as effective building blocks to construct versatile nanostructures of various sizes and shapes.[40−43] However, unlike the traditional carrier-based drug delivery strategies where the carriers can be constructed from a great diversity of molecular building units, the use of a drug to build nanocarriers of its own is limited by the molecular design and synthetic feasibility. It is therefore necessary to seek other assembly strategies to access different morphologies required for controlled delivery properties under various conditions.

Co-assembly of two or more different amphiphilic molecules is one such strategy that can be used to influence both the functional and structural properties of the nanostructures formed. For example, it has been shown that mixing of amphiphiles with opposite charges provides a means for controlling the surface charge of the assembly through variation of the mixing ratio and can be used to introduce multiple functionalities if the two amphiphiles being coassembled have differing epitopes.[44−47] These catanionic mixtures (CAMs) can also possess intriguing phase behaviors and usually offer alternative morphologies compared with that formed by each individual amphiphile.[48,49] It is generally believed that the formation of ion pairs by oppositely charged surfactants reduces the electrostatic repulsions among the headgroups, leading to a reduced curvature to form bilayered assemblies.[50] This strategy of mixing two oppositely charged amphiphilic molecules has been used to produce a variety of bilayered nanostructures, including vesicles,[48,49,51] icosahedra,[52] nanodiscs,[53] and nanobelts.[47] Tubular structures, which can be considered as curved bilayer architectures, are rarely reported in catanionic systems.[54] We show here that catanionic mixtures of two drug amphiphiles (DAs)—each with a 36% fixed loading of the anticancer drug camptothecin (CPT)—lead to formation of a multiwalled nanotube morphology that also possesses a 36% fixed CPT loading.

RESULTS AND DISCUSSION

The DAs used in this study were designed to contain either one, two, or four hydrophobic CPTs that are conjugated to a β-sheet-forming peptide sequence through a reducible disulfylbutyrate (**buSS**) linker (Figure 1a and Scheme S1, Supporting Information).[34] The peptide segments with *N*-terminal cysteine residues were first synthesized using standard Fmoc solid-phase peptide synthesis protocols. The conjugation of the peptide with the CPT units was carried out in DMSO, utilizing a direct disulfide formation approach in which the peptide cysteine(s) displace thiopyridinone from **CPT-buSS-Pyr** (see section S1 in the Supporting Information for details). The peptide moiety GNNQQNY is a key β-sheet forming sequence derived from the yeast prion Sup35[55] and was chosen to afford the capacity for intermolecular hydrogen bonding between the designed DAs. Two lysine (**K**) or two glutamic acid (**E**) residues were placed at the *C*-terminal of the studied peptide to imbue both the overall amphiphilicity and the charge status (positive or negative). The main DA of interest, **qCPT-Sup35**, possesses four CPTs that are chemically bonded to the peptide moiety, giving a fixed drug loading of 36% (see the Supporting Information, S1). Both the *C*-terminal **K** and **E** DAs were synthesized, furnishing **qCPT-Sup35-K_2** and **qCPT-Sup35-E_2**, respectively.

Catanionic Assembly. To ensure molecular level mixing of DAs and to preclude possible preassembled structures, the CAMs were prepared using the following procedure: first, each molecule was dissolved in hexafluoroisopropanol (HFIP)—a solvent that is disruptive toward the formation of assembled structures for all the studied molecules. Next, two solutions containing the respective molecules were mixed at the desired molar ratio, followed by lyophilization of the mixed solution. The lyophilized material was then dissolved in 1:1 MeCN/H_2O to a desired concentration, aged overnight, and subsequently imaged by cryogenic transmission microscopy (cryo-TEM). Cryo-TEM enables the direct visualization of the assembled structures in vitrified water, minimizing artifacts that can result from the drying and staining of samples in conventional TEM.[56]

Morphology Characterization. At 400 μM, the CAMs formed by **qCPT-Sup35** revealed dominant tubular structures when mixed at a 1:3 ratio of amine to carboxylic acid (1:3 for the following notations) in 1:1 MeCN/H_2O after aging overnight (Figure 1d−f). The two-dimensional projection of a tubular structure in cryo-TEM imaging differs from other types of self-assembled construct, showing two parallel, darker lines at the edges and a shady span in the tubular body. This contrast can be attributed to the high electron density of the densely packed hydrophobic core and the relatively longer traveling distances of the electrons through the nanotube edges. In contrast, the individual DAs were found to assemble into filamentous nanostructures (~6 nm in diameter in both cases), when reconstituted in 1:1 MeCN/H_2O using the exact HFIP-pretreatment protocols (Figure 1b,c; further discussions of the supramolecular structures formed by the individual DA are provided in the Supporting Information). This clearly suggests that it is the mixing of the cationic and anionic forms of **qCPT-Sup35** that gives rise to the tubular morphology.

These observed tubular structures in CAM solutions possess outer diameters of ~123 nm and wall thickness up to ~25 nm (measured from cryo-TEM

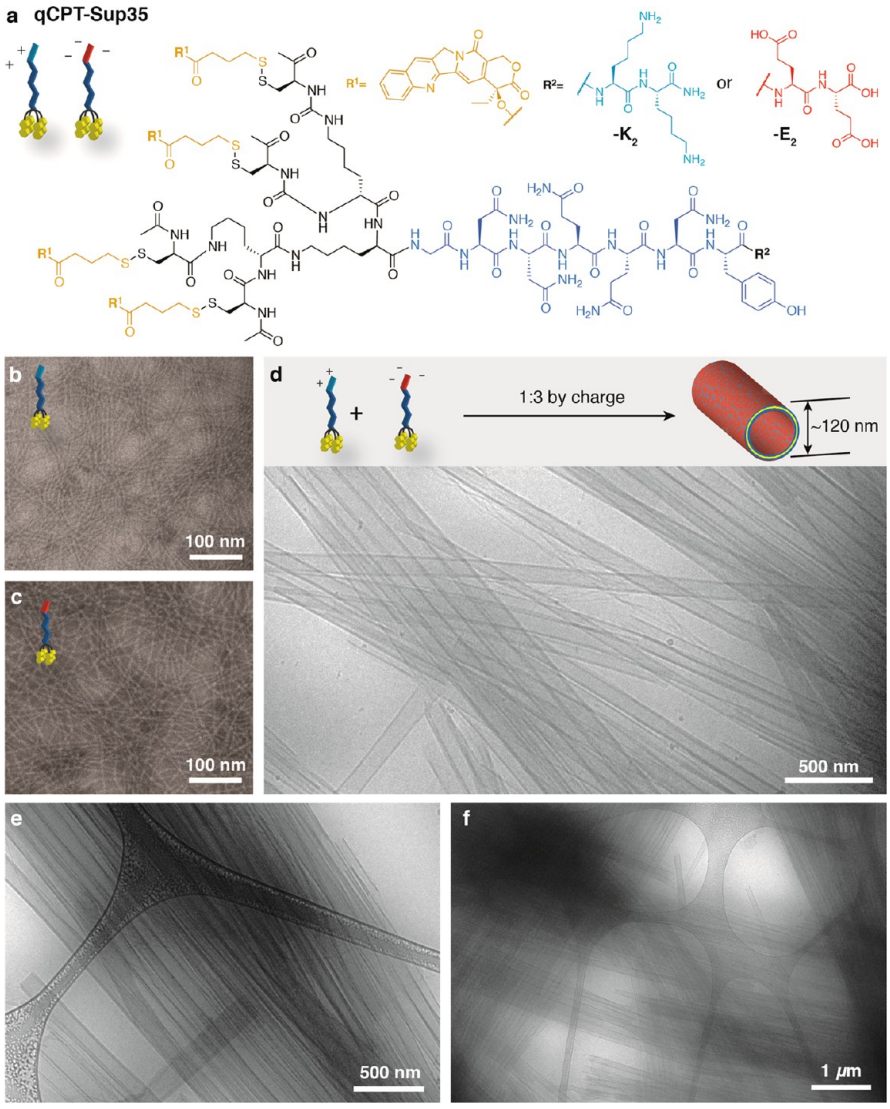

Figure 1. (a) Chemical structures and schematic representations of qCPT-Sup35-K_2 and qCPT-Sup35-E_2. (b–d) Schematic representations and TEM micrographs of the supramolecular structures formed by qCPT-Sup35-K_2, qCPT-Sup35-E_2, and the CAM of the two DAs. Both qCPT-Sup35-K_2 (b) and qCPT-Sup35-E_2 (c) formed single filaments in 1:1 MeCN/H_2O after the materials had been previously treated with HFIP. The widths of the single filaments measured from TEM are 5.7 ± 0.9 nm, and 5.9 ± 0.9 nm for qCPT-Sup35-K_2 and qCPT-Sup35-E_2, respectively. (d–f) The CAM of qCPT-Sup35 (mixing ratio 1:3) results in the almost exclusive formation of tubular structures in 1:1 MeCN/H_2O. The tubular size measured from cryo-TEM imaging is 123 ± 28 nm. Total concentration for all samples = 400 μM.

micrographs). Assuming the **qCPT-Sup35** CAMs form a single bilayer, the maximum shell thickness would be comparable to twice the extended length of the individual DAs, approximately 10 nm. Thus, the greater wall thickness observed in cryo-TEM micrographs (~25 nm *vs* ~10 nm) suggests the presence of multiple bilayers in some assembled structures. Indeed, multi-walled constructs could be occasionally observed in cryo-TEM imaging (Figure 2a,b), providing direct support for this inference.

Another interesting observation of these nanotubes in cryo-TEM imaging is their remarkable tolerance to deformation. We first observed irregular undulations in the tube diameter (Figure 2c,d and Figure S9a, Supporting Information). The broadening of the tubular diameter did not display any periodic pitch and generally occurred in regions where the tubules overlapped with other nanotubes or with the lacey carbon film. We therefore speculate that this "squeezing" of the tubules may be a result of being confined into the thin vitreous water layer (typically less than ~250 nm[56]) that were generated in the cryo-TEM sample preparation. Occasionally, it could be spotted that the otherwise straight nanotubes were bending, appearing as a "folded straw" structure in which pinching of the tube was seen at the bend point (Figure 2a–c). Surprisingly, this bending did not lead to the breakdown of the tubular structures unless the angle of bending exceeded 90°, and even then the two sections still remained connected (Figure 2b). Both observations

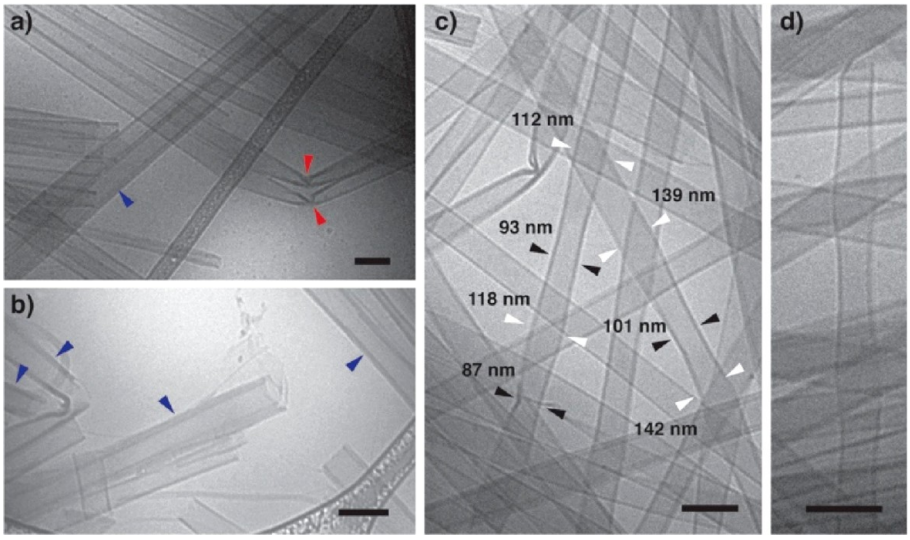

Figure 2. TEM and cryo-TEM micrographs of the qCPT-Sup35 CAM with a mixing ratio of 1:3 at 400 μM in 1:1 MeCN/H_2O. (a, b) Bending of the tubular structures (indicated by the red arrows) and the direct observation of the multiwalled nature of the tubules (labeled with blue arrows) in cryo-TEM imaging. (c, d) Undulation of the tube widths is commonly observed in regions where overlapping occurs. All bars = 200 nm.

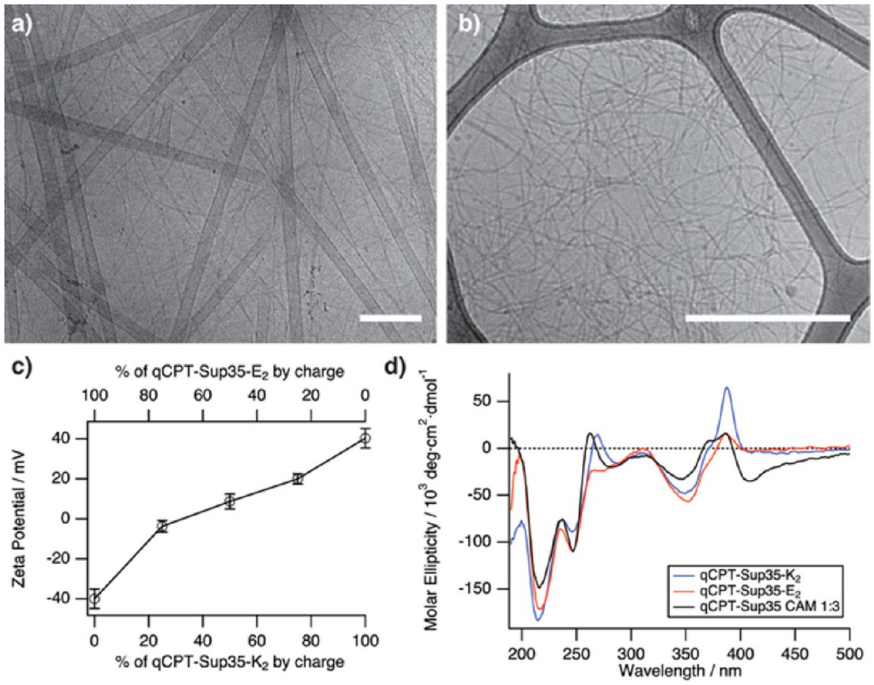

Figure 3. (a, b) Cryo-TEM micrographs of qCPT-Sup35 CAMs with a mixing ratio of 1:1 (a) and 3:1 (b) at 400 μM in 1:1 MeCN/H_2O. All bars = 500 nm. (c) Zeta potential measurements of the qCPT-Sup35 CAMs with different mixing ratios. Data are presented as mean $\pm$ s.d. (d) CD spectra of the 1:3 qCPT-Sup35 CAM, and individual DAs in 1:1 MeCN/H_2O. All spectra were obtained from 400 μM solutions that were diluted to 50 μM immediately prior to measurement.

imply that molecular packing within these tubules is reminiscent of that of fluidic-like bilayers. The tolerance that the CPT nanotubes demonstrated under deformation is in sharp contrast with reported tubular morphologies that often have a brittle, well-ordered internal packing.[11,24]

We found that the overall mixing ratio plays a critical role in defining the final assembled morphologies. Dominant tubular structures were only observed for mixing ratios of 1:3−1:5 (amine to carboxylic acid) at the concentration of 400 μM. Zeta potential measurements reveal that these nanotubes remain almost neutral on their surface (−3.79 $\pm$ 2.86 mV for **qCPT-Sup35** CAM 1:3) (Figure 3c); this may imply most of the amphiphiles formed ion pairs so that the charges were nearly neutralized. Increasing the amount of **qCPT-Sup35-K_2** in the mixture to give a 1:1 ratio of amine to carboxylic acid, however, led to the coexistence

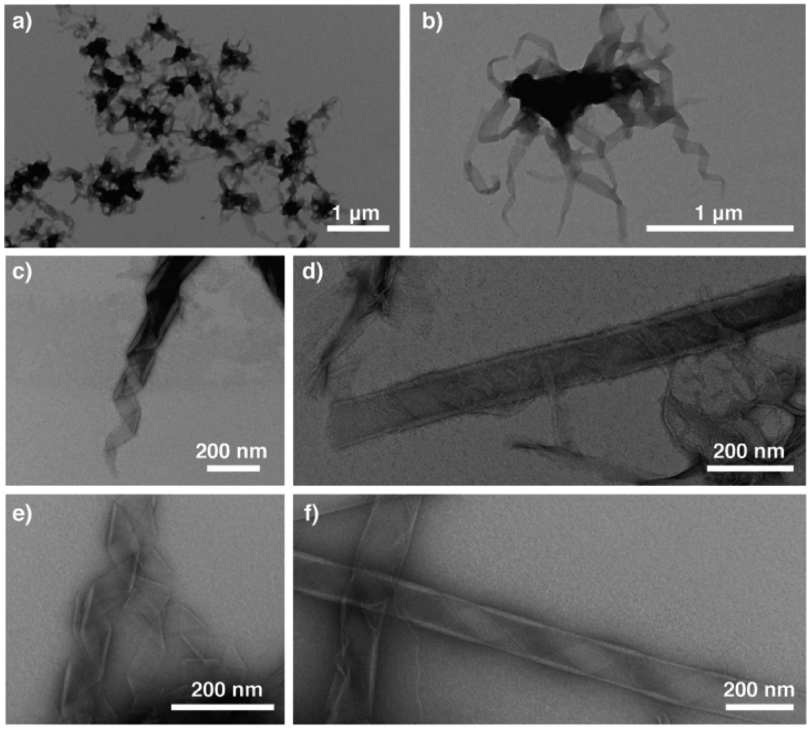

Figure 4. TEM micrographs of the intermediate structures of the 1:3 qCPT-Sup35 CAM in 1:1 MeCN/H_2O, unless stated otherwise. (a, b) Clusters of belts and helical ribbons are the dominant structures at 10 μM (a) and 50 μM (b). (c) Multilayer helical ribbon at 50 μM. (d) An intermediate multiwall tubular structure in a 100 μM solution, showing a tubular structure wrapped with another layer of belt. (e, f) Similar intermediate structures, such as multilayer helical ribbons and intermediate multiwall tubular structures in 3:1 MeCN/H_2O, where the materials exhibited limited solubility. Bulk concentration = 400 μM.

of tubules and filamentous structures (Figure 3a; zeta potential: 8.68 $\pm$ 3.79 mV). As the content of **qCPT-Sup35-K_2** was raised to yield a mixing ratio of 3:1, filamentous structures started to dominate; large tubules could still be observed but displayed a significant decrease in length (on the order of a few μm) (Figure 3b and Figure S9f, Supporting Information).

Circular dichroism (CD) spectroscopy provides additional insight into the secondary structure of the peptide domain of the DAs and also into the environment of the CPT moieties. Analysis of the 1:3 **qCPT-Sup35** CAM in 1:1 MeCN/H_2O reveals a number of interesting signals (Figure 3d). First, a strong negative peak at 215 nm can be seen, a characteristic indicator of the β-sheet conformation that is in agreement with the one-dimensionality of the assembled structures. Second, signals from the CPT moieties are also evident, displaying a negative signal at 250 nm (n$-\pi^*$) and a series of signals between 330 and 500 nm ($\pi-\pi^*$) that are caused by the chiral packing of CPT moieties in the assembled form. Third, the lack of any truly bisignate peaks suggests that the CPT molecules may be aligned in a parallel fashion, rather than with a helical sense as was previously observed in the Tau peptide analogue.[34] Comparison with the CD spectra of the individual DAs under the same assembly conditions shows there are some similarities in the peptide absorption region with the major difference in the CPT absorption regions—the tubes having a very broad negative signal between 400 and 500 nm (Figure 3d). The exact origin of this peak is unclear but may be linked to the formation of the nanotubes, given the fact that this peak also appears in the CD spectra of CAMs with different mixing ratios that exhibit the tubular structures (Figure S10, Supporting Information). These results clearly suggest that it is the arrangement of CPT units that is primarily responsible for the formation of the tubular morphology.

Nanotube Assembly Pathways. Observations of intermediate structures often provide evidence for the mechanistic pathway and kinetic processes that engender the formation of large structures like nanotubes. This information can be obtained by variation of assembly conditions such as concentration and solvents. We found that the dominant supramolecular morphology for **qCPT-Sup35** CAM 1:3 is strongly dependent upon two factors—the bulk concentration and the MeCN/H_2O ratio. In the case of the former, we found that intermediate structures could be seen at lower concentrations in 50% MeCN (Figure 4a–d). At 10 μM, clusters of beltlike structures were more commonly observed (Figure 4a,b). As the bulk concentration was increased to 50 or 100 μM, more complex assemblies such as helical ribbons (Figure 4c) and ribbon-wrapped tubes appeared (Figure 4d). The pitch angle of these helical ribbons is consistently close to 45°, a feature predicted theoretically in curved membranes that form helical ribbons or tubules characterized by

chiral packing.[57,58] In addition, the ribbon-wrapped tubes provide direct evidence for the multiwalled nature of these tubules, accounting for the tubular thickness variation observed at higher concentrations. It is noted that the observed ribbons display attenuating widths gradually at the ends with a fixed pitch, implying that formation of the tubules results from widening of ribbons rather than from the shrinking of helical coils (Figure 4b,c).

Variation of the solvent composition was found to have a similar effect on the self-assembly of **qCPT-Sup35** CAMs 1:3. It was found that the CAMs could not be directly reconstituted in pure water after the HFIP treatment, instead suffering from low material solubility that did not lead to the formation of any well-defined structures. Similarly, the **qCPT-Sup35** CAMs also exhibited poor solubility in pure MeCN, immediately forming huge precipitates with no well-defined structures observed by TEM. Though a **qCPT-Sup35** CAM gave a turbid solution when reconstituted in 3:1 MeCN/H_2O at 400 μM, intermediate structures could still be observed in TEM imaging, exhibiting similar multilayered helical ribbon and ribbon-wrapped tubule structures to those discovered at 50 or 100 μM when using 1:1 MeCN/H_2O as solvent (Figure 4e,f). Again, both types of intermediate structures are indicative of at least two independent growth pathways for the studied system: multilayer formation and tubular formation from helical ribbons.

Role of Molecular Design. In order to further explore the role that the CPT unit plays in the formation of nanotubes, we prepared CAMs for **mCPT-Sup35** and **dCPT-Sup35** possessing one and two CPT molecules, respectively, under exactly the same conditions to produce **qCPT-Sup35** nanotubes. In the case of catanionic mixing of **mCPT-Sup35-K_2** and **mCPT-Sup35-E_2** in 1:1 MeCN/H_2O at 400 μM, well-defined structures were only scarcely observed. The CAM of **dCPT-Sup35** exhibited exclusively 1D filamentous structures in 1:1 MeCN/H_2O at 400 μM regardless of the mixing composition tested (mixing ratio of amine to carboxylic acid: 1:3, 1:1, or 3:1, see Figure S11, Supporting Information), similar to those observed for the individual DAs of **qCPT-Sup35**. CD spectra of **dCPT-Sup35** CAM, **dCPT-Sup35-K_2**, and **dCPT-Sup35-E_2** all display a negative peak at ~215 nm that corresponds to the β-sheet secondary structure and signals from the CPT chromophores in the 260−410 nm range (Figure S12, Supporting Information). The fact that few differences in the CD were detected for the CAMs of **dCPT-Sup35** when compared with the individual components suggests there is no change in the packing arrangement of the CPT molecules upon CAM formation, especially considering the occurrence of the negative signal in the 400−500 nm range that was observed for the **qCPT-Sup35** CAMs. Consequently, the packing requirements of the hydrophobic core within the assemblies formed by CAMs of **qCPT-Sup35** must play a crucial role for the mixtures to adopt tubular structures as their dominant supramolecular morphology (Figure 5a).

These results suggest the molecular mixing ratio, the solvent composition, the overall concentration, as well as the molecular structures of the studied drug amphiphiles are all important experimental factors to define the tubular morphology. On the basis of our observation of the intermediate helical ribbons, the most plausible kinetic pathway to form these observed multiwalled nanotubes by **qCPT-Sup35** CAM is the widening of the helical ribbons that are composed of multiple bilayered structures. The forming process is likely a cumulative result of 1D elongation, multiple bilayer formation, and bilayer extension (Figure 5b).

We speculate that both bilayer formation (packing geometry) and chiral stacking (packing directions) play a key role in the formation of nanotubes reported here. The importance of the bilayer formation is supported by the observations that only **qCPT-Sup35** CAMs can form the tubular morphology. Both **mCPT-Sup35** and **dCPT-Sup35** CAMs form filamentous nanostructures under the same conditions. Several CAM systems suggest that catanionic mixing of sphere or cylinder-forming amphiphiles could produce bilayered structures.[48,51−53] This can also be used to reasonably explain our studied system. Neither the CAMs of **mCPT-Sup35** and **dCPT-Sup35** nor individual **qCPT-Sup35-K_2** and **qCPT-Sup35-E_2** could satisfy the requirement for a bilayer packing geometry due to either the relatively smaller hydrophobic segments or the relatively large headgroup areas. The multiwalled construct is reminiscent of multilamellar vesicles commonly observed in concentrated catanionic mixtures.[48] This stacking is known to be driven by short-range interactions, such as attractive van der Waals interaction, electrostatic interactions, hydration force, and attractive hydrophobic interactions.[48,59] The observation of helical ribbons as the nanotube precursor morphology strongly suggests the formation of tubular structures in our system shares some common features with the lateral extension of helical ribbons into tubules of chiral self-assemblies that have been reported by other laboratories.[15,23,60−64] We speculate that the chiral packing in our system stems from the Sup35 peptide segment but is also affected by the stacking among the CPT units. However, it is difficult to deconvolute the contribution of the CPT interaction from hydrogen bonding in our system for the formation of nanotubes, given the fact that $\pi-\pi$ interactions among the CPT moieties are also known to lead to 1D chiral structures.

***In Vivo* Evaluation.** Since these catanionic nanotubes contain a 36% fixed loading of the anticancer drug CPT, we performed preliminary studies to investigate if CPT nanotubes present any advantageous properties over the free drug for use as drug vehicles. We first

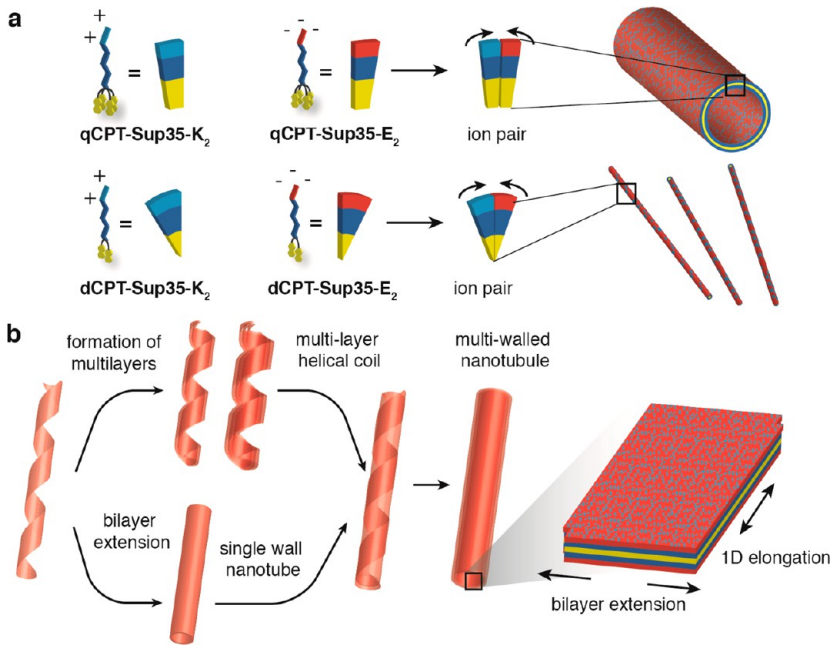

Figure 5. Proposed mechanism of the tubule formation by qCPT-Sup35 CAMs. (a) Schematic illustration of the effect of packing parameter of qCPT-Sup35 and dCPT-Sup35 on the formation of ion pairs and the resulting supramolecular morphology of corresponding catanionic mixtures. (b) The formation of the multiwall nanotubes by CAMs of qCPT-Sup35 is the cumulative result of three occurrences: 1D elongation, formation of multilayers, and bilayer extension from helical ribbons. The CAM of qCPT-Sup35 formed bilayers, where the direction of lateral bilayer extension is perpendicular to the orientation of the intermolecular hydrogen bonds.

evaluated their potential for local delivery on CT26 tumor-bearing mice. The CPT nanotubes were labeled with a near-infrared dye Cy7.5 (5% loading by mol), and the labeled material was directly injected into the tumor sites, with the free Cy7.5 as control. The distribution of the nanotubes at different time points was monitored using near-infrared fluorescence (NIRF) imaging. It can be seen that the labeled nanotubes mostly stayed in the tumor tissue even after 36 h following intratumoral injection (Figure S13, Supporting Information). In contrast, a considerable amount of free Cy7.5 was already eliminated from the tumor tissue after only 2 h (Figure 6a,b). Clearly, the significantly enhanced retention time of CPT nanotubes in the tumor site offers the possibility for sustainable release of CPT over a long period of time that would be beneficial for local tumor treatment. However, systemic delivery of CPT nanotubes through tail-vein injection did not show any improvement for tumor targeting. We found that most injected CPT nanotubes quickly accumulated in the liver (about 5 min) and were gradually eliminated within 24 h (Figure S14, Supporting Information). We believe that the inability of CPT catanionic nanotubes to circulate through the liver may be attributed to their relatively large size and the negatively charged surface chemistry that promote serum protein adsorption and liver entrapment. Given the previous reports on the prolonged circulation time of filamentous nanostructures by Discher and co-workers[65] and the low protein adsorption of zwitterionic material by

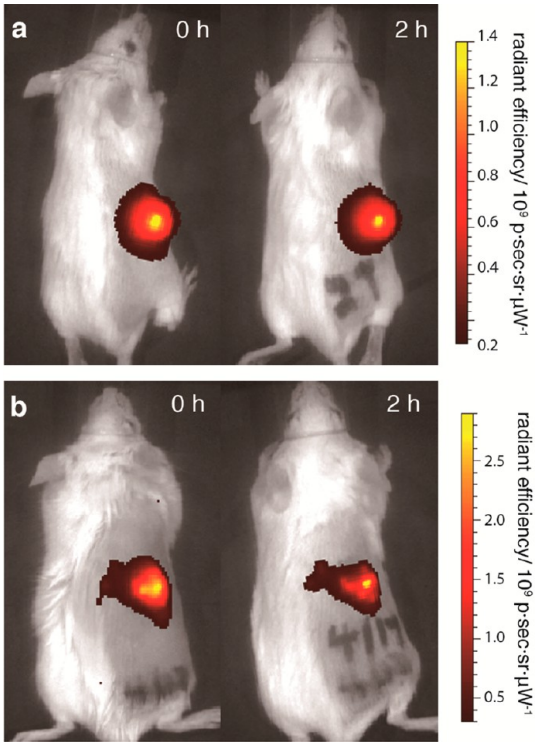

Figure 6. *In vivo* NIRF imaging of CT26 tumor-bearing mice. The heat maps display the distribution of Cy7.5 labeled CAM nanotubes of qCPT-Sup35 (a) and free Cy7.5 (b) after intratumoral injection.

Jiang and co-workers,[66] we are optimistic that after further modification and optimization of the size and surface chemistry these CPT nanotubes could be

tailored with suitable physicochemical properties for systemic delivery.

CONCLUSION

In summary, we have successfully utilized the CAMs of therapeutic DAs to form tubular constructs with multiwalled architectures. Our results reveal that such structures are formed through the combination of 1D elongation and bilayer extension that is induced by a significant reduction in curvature as a result of catanionic mixing. Our findings provide insight into the construction of tubules with interesting properties through the self-assembly of catanionic mixtures. In particular, our preliminary animal experiments showed that these CPT nanotubes could be used as a local depot for sustainable release of CPT drugs.

MATERIALS AND METHODS

Peptide Synthesis. The peptides utilized in this study were synthesized employing standard Fmoc solid-phase protocols, using either Rink Amide MBHA or Fmoc-Glu(tBu)-Wang resins at a 0.25 mmol synthesis scale. An automated peptide synthesizer (Focus XC, AAPPTec, Louisville, KY) was employed to build the Sup35 sequence before manual protocols were used to furnish the branching motif. Fmoc deprotection of the Fmoc-amino acids was established by treating the resin with 4-methylpiperidine in dimethylformamide (DMF) (20% v/v). The amino acid coupling cycle was performed after Fmoc deprotection, and the resin was treated with Fmoc-amino acids, *O*-benzotriazole-*N*,*N*,*N*′,*N*′-tetramethyluronium hexafluorophosphate (HBTU), and diisopropylethylamine (DIEA) (4:4:6 molar equiv to resin) in DMF for 1 h. The branching molecular design was achieved by coupling Fmoc-Lys(Fmoc)-OH at the N-terminus to yield multiple primary amine groups after Fmoc-deprotection for the further coupling of Fmoc-Cys(Trt)-OH in a branch construct. The N-termini of the peptides were acetylated with 20% acetic anhydride in DMF. Peptides were then cleaved from the resin by trifluoroacetic acid (TFA)/triisopropylsilane (TIS)/1,2-ethanedithiol (EDT)/ H2O (92.2:2.5:2.5:2.5) for 2 h. The liquid residue was concentrated *in vacuo* and added into ice-cold Et_2O to yield pale precipitates. These crude peptides were then filtered, collected, kept in the desiccator to remove the remaining solvent, and directly used for the following reaction.

Synthesis of 4-(Pyridin-2-yldisulfanyl)butanoic Acid. This was synthesized by a modified protocol based on previously reported work.[67] In brief, 4-bromobutyric acid (2.0 g, 12.0 mmol) and thiourea (1.06 g, 14.0 mmol) were refluxed in ethanol (50 mL) for 4 h. After addition of NaOH (4.85 g, in 10 mL of EtOH) into this solution, the mixtures was refluxed for an additional 16 h. After the solution was cooled to room temperature, it was concentrated *in vacuo*, and diluted with water and extracted twice with ethyl ether. The aqueous phase was then acidified by 4 M HCl to pH 5, resulting in a cloudy solution that was extracted by ethyl ether. The organic portion was dried with Na_2SO_4 and concentrated to yield clear, oil-like 4-sulfanylbutyric acid. 4-Sulfanylbutyric acid was then dissolved in MeOH and added dropwise into a 5 mL methanolic solution of 2-aldrithiol (3.03 g, 0.0137 mol). The mixtures were allowed to react for 3 h and were purified by RP-HPLC. Purified products were collected and solvents removed *in vacuo*. The resultant yellowish oil was then dissolved in $CHCl_3$ and dried over Na_2SO_4 and solvent removed to give HO_2C-buSS-Pyr as a light yellow oil. ^1H NMR ($CDCl_3$, 400 MHz, 298 K): δ_H (ppm) 8.59 (d, $^3J_{HH}$ = 4.6 Hz, 1H), 7.91−7.81 (m, 2H), 7.30−7.25 (m, 1H), 2.88 (t, $^3J_{HH}$ = 7.1 Hz, 2H), 2.50 (t, $^3J_{HH}$ = 7.2 Hz, 2H), 2.09−2.00 (m, 2H).

Synthesis of Camptothecin-4-(pyridin-2-yldisulfanyl)butanoate (CPT-buSS-Pyr). Camptothecin (CPT, 200 mg) and (dimethylamino)-pyridine (DMAP, 44 mg) were initially suspended in DCM (32 mL). HO_2C-buSS-Pyr (280 mg) and diisopropylcarbodiimide (DIC, 436 μL) were then added to the mixture and the resulting solution stirred for 36 h. This solution was then filtered, diluted with chloroform (60 mL), washed with sat. $NaHCO_3$ (50 mL) and brine (50 mL), dried over Na_2SO_4, and concentrated *in vacuo*. The crude product was purified by flash chromatography using EtOAc (500 mL) and then 0.5% MeOH in EtOAc (250 mL). Collected products were identified by TLC and underwent solvent removal *in vacuo* to yield a yellow solid. ^1H NMR ($CDCl_3$, 400 MHz, 298 K): δ_H (ppm) 8.43 (d, $^3J_{HH}$ = 4.2 Hz, 1H), 8.40 (s, 1H), 8.23 (d, $^3J_{HH}$ = 8.6 Hz, 1H), 7.94 (d, $^3J_{HH}$ = 8.2 Hz, 1H), 7.84 (m, 1H), 7.70−7.65 (m, 2H), 7.60 (m, 1H), 7.20 (s, 1H), 7.04 (m, 1H), 5.67 (d, $^2J_{HH}$ = 17.3 Hz, 1H), 5.40 (d, $^2J_{HH}$ = 17.2 Hz, 1H), 5.29 (s, 2H), 2.86 (t, $^3J_{HH}$ = 7.1 Hz, 2H), 2.75−2.57 (m, 2H), 2.31−2.03 (m, 4H), 0.97 (t, $^3J_{HH}$ = 7.5 Hz). ^{13}C NMR ($CDCl_3$, 100 MHz, 298 K): δ_C (ppm) 172.1, 167.7, 160.3, 157.6, 152.6, 149.9, 149.1, 146.6, 146.1, 137.3, 131.5, 131.4, 130.9, 129.9, 128.63, 128.62, 128.4, 128.3, 120.4, 96.1, 76.2, 67.4, 50.2, 37.7, 32.4, 32.0, 31.2, 24.0, 7.9. MS (MALDI-TOF): 560.065 $[M + H]^+$.

Syntheses of the DAs and Purification. The syntheses of all DAs were carried out by dissolving CPT-buSS-Pyr and the corresponding crude peptides in N_2-purged dimethyl sulfoxide (DMSO, 1 mL) (2:1 by mol). The mixtures were allowed to react for 5 d at room temperature, and the resulting solutions were diluted by MeCN/H_2O and then purified by RP-HPLC. Eluted products after purification were collected, flash frozen by liquid nitrogen, and lyophilized. The purity of the collected products was confirmed by RP-HPLC and ESI-MS, and the conjugate concentrations were calibrated before being aliquotted into predetermined amounts.

Calibration of the Concentration. The concentration of DAs was calibrated by analyzing the reduced product from the DAs−CPT-buSH. A stock solution of the DA was prepared by dissolving in MeCN/H_2O (1:1). A 5 μL portion of the stock DA solution was then diluted to 20 μL by MeCN/H_2O (1:1) and mixed with 20 μL of 1 M tris(2-carboxyethyl)phosphine (TCEP) for 45 min. The resultant solution was then analyzed by RP-HPLC, monitoring the absorbance at 370 nm. The CPT concentration of the analyte solution was then calculated from the area under the curve in the chromatogram by comparison with the standard solutions based on the content of CPT-buSH. The conjugate concentration of the stock solution was then determined on the basis of the applied dilution and the number of CPT molecules.

Preparation of the Catanonic Mixtures (CAMs). The two components of the CAMs were dissolved in hexafluoro-2-propanol (HFIP) separately to yield clear solutions. The CAMs were prepared by mixing the two DAs that were dissolved in HFIP, with mixing ratios of 1:3, 1:1, or 3:1 (ratio of amines to carboxylic acids), while the total peptide amount was kept constant in each vial (by mole). The mixtures were then flash frozen in liquid nitrogen and lyophilized to yield dry solids. Solutions were then reconstituted in 1:1 MeCN/H_2O and aged overnight for further studies.

Transmission Electron Microscopy (TEM). The TEM samples were prepared by negative staining techniques. The solutions (7 μL) were initially loaded on copper grids covered with carbon film. The liquids were then removed by filter papers, and 2% uranyl acetate solutions (7 μL) were subsequently deposited on the samples. The uranyl solutions were then removed by filter paper blotting after 30 s. The specimens were air-dried prior to imaging. Bright-field TEM imaging was performed on an FEI Tecnai 12 TWIN electron microscope at 100 kV. The micrographs were acquired by a SIS Megaview III wide angle camera.

Cryogenic-Transmission Electron Microscopy (Cryo-TEM). Specimens of cryo-TEM imaging were prepared by Vitrobot (FEI, Hillsboro, OR). The solutions were initially loaded on a copper grid with Lacey carbon film (Electron Microscopy Sciences, Hatfield, PA) in the controlled humidity chamber and were blotted by the filter

papers that were mounted on the Vitrobot from both sides of the grid. This process engenders a thin film of solutions that adhere on the sample grid. The blotted samples were then transferred into liquid ethane and were stored in liquid nitrogen until further use. Sample imaging was conducted on a FEI Tecnai 12 TWIN electron microscope at 100 kV. The micrographs were acquired by a 16 bit 2K × 2K FEI Eagle bottom mount camera.

Circular Dichroism Spectroscopy. The CD spectra were monitored by using a JASCO J-710 spectropolarimeter (JASCO, Easton, MD). Solutions were loaded in 1 mm cuvettes, and the spectra were recorded in the far-UV and vis region. The molar ellipticity was calculated by the following equation

$$[\theta] = \theta/cl$$

where $[\theta]$ represents the molar ellipticity, θ is the measured ellipticity in deg, c is the concentration of the DAs in dmol·cm^{-3}, and l is the light path length of the cuvette in cm.

Zeta Potential Measurements. The zeta potential measurements were performed on a Zetasizer Nano ZS90 (Malvern Instruments Ltd., UK). The prepared solutions were loaded in folded capillary cells and equilibrated for 2 min prior to measurements. The zeta potential of the assembled structures was obtained by measuring the electrophoretic movement of the nanostructures under the applied electric field, where the movement velocity is determined by phase analysis light scattering.

Animal Model. All experiments conducted with mice were performed in accordance with protocols approved by the Johns Hopkins University Institutional Animal Care and Use Committee (IACUC). CT26 (CRL-2638) murine colorectal adenocarcinoma cells were purchased from the American Type Culture Collection (ATCC) and grown in McCoy's 5A medium (Invitrogen/Life Technologies, Carlsbad, CA) supplemented with 10% fetal bovine serum (FBS, HyClone, Thermo Scientific, Waltham, MA) at 37 °C with 5% CO2. Five million CT26 cells were injected subcutaneously into the right flank of female BALB/c mice (6−8 weeks; Harlan, Indianapolis, IN; ∼20 g in weight) and allowed to grow for ∼10 days.

Near-IR Imaging *in Vivo*. Nanotubes formed by CAM of **qCPT-Sup35** was labeled with Cy7.5 for near-IR imaging. In brief, **qCPT-Sup35-K$_2$** (45 nmol) was mixed with Cy7.5-NHS ester (90 nmol, Lumiprobe, Hallandale Beach, FL) in DMSO (300 μL) and reacted at room temperature for 48 h. This solution was then diluted with H_2O/MeCN (1:1) and purified by RP-HPLC. Eluted product was collected and then lyophilized to yield the dry mass of **Cy7.5-qCPT-Sup35-K$_2$**. Specimens of CAM of **qCPT-Sup35** 1:3 were then prepared by mixing **qCPT-Sup35-K$_2$**, **Cy7.5-qCPT-Sup35-K$_2$**, and **qCPT-Sup35-E$_2$** in HFIP with a labeling percentage at 5% (by mol). The CAMs in FHIP were then lyophilized and reconstituted by H_2O/MeCN (1:1) 30 min prior to the usage for injection. The animal was administered with 20 μL of a 500 μM solution when the injection took place at the tumor tissue or with 200 μL of a 500 μM solution when performing tail injection. Fluorescence imaging was performed and analyzed by using an IVIS Spectrum/CT *in vivo* imaging system with the Living Image software (PerkinElmer, Waltham, MA). Fluorescence signal (emission = 800 nm, excitation = 780 nm) was quantified as radiant efficiency.

Conflict of Interest: The authors declare no competing financial interest.

Supporting Information Available: Additional molecular characterization, spectroscopic studies, and additional TEM images. This material is available free of charge *via* the Internet at http://pubs.acs.org.

Acknowledgment. We acknowledge financial support from the National Science Foundation (DMR 1255281) and the National Institutes of Health for funding Y.L. (R25CA153952) and A.C. (T-32CA130840). G.L. acknowledges the financial support from National Institutes of Health (R21EB015609). We also acknowledge JHU Integrated Imaging Center (IIC) for TEM imaging, Prof. K. Hristova (JHU MSE) for the use of the CD spectropolarimeter, and the NSF (NSF CHE-0840463) for the purchase of a mass spectrometer at the the JHU Department of Chemistry.

REFERENCES AND NOTES

1. Hill, J. P.; Jin, W. S.; Kosaka, A.; Fukushima, T.; Ichihara, H.; Shimomura, T.; Ito, K.; Hashizume, T.; Ishii, N.; Aida, T. Self-Assembled Hexa-peri-hexabenzocoronene Graphitic Nanotube. *Science* **2004**, *304*, 1481–1483.
2. Iijima, S. Helical Microtubules of Graphitic Carbon. *Nature* **1991**, *354*, 56–58.
3. Treacy, M. M. J.; Ebbesen, T. W.; Gibson, J. M. Exceptionally High Young's Modulus Observed for Individual Carbon Nanotubes. *Nature* **1996**, *381*, 678–680.
4. Mitchison, T.; Kirschner, M. Dynamic Instability of Microtubule Growth. *Nature* **1984**, *312*, 237–242.
5. Hamley, I. W. Peptide Nanotubes. *Angew. Chem. Int. Ed.* **2014**, *53*, 6866–6881.
6. Zhang, W.; Jin, W. S.; Fukushima, T.; Saeki, A.; Seki, S.; Aida, T. Supramolecular Linear Heterojunction Composed of Graphite-Like Semiconducting Nanotubular Segments. *Science* **2011**, *334*, 340–343.
7. Adler-Abramovich, L.; Aronov, D.; Beker, P.; Yevnin, M.; Stempler, S.; Buzhansky, L.; Rosenman, G.; Gazit, E. Self-Assembled Arrays of Peptide Nanotubes by Vapour Deposition. *Nat. Nanotechnol.* **2009**, *4*, 849–854.
8. Gazit, E. Self-Assembled Peptide Nanostructures: The Design of Molecular Building Blocks and Their Technological Utilization. *Chem. Soc. Rev.* **2007**, *36*, 1263–1269.
9. Ashkenasy, N.; Horne, W. S.; Ghadiri, M. R. Design of Self-Assembling Peptide Nanotubes with Delocalized Electronic States. *Small* **2006**, *2*, 99–102.
10. Zhang, J.; Liu, X.; Blume, R.; Zhang, A. H.; Schlogl, R.; Su, D. S. Surface-Modified Carbon Nanotubes Catalyze Oxidative Dehydrogenation of n-Butane. *Science* **2008**, *322*, 73–77.
11. Schnur, J. M. Lipid Tubules - A Paradigm for Molecularly Engineered Structures. *Science* **1993**, *262*, 1669–1676.
12. Margulis-Goshen, K.; di Gregorio, M. C.; Pavel, N. V.; Abezgauz, L.; Danino, D.; Tato, J. V.; Tellini, V. H. S.; Magdassi, S.; Galantini, L. Drug-Loaded Nanoparticles and Supramolecular Nanotubes Formed from A Volatile Microemulsion with Bile Salt Derivatives. *Phys. Chem. Chem. Phys.* **2013**, *15*, 6016–6024.
13. Stewart, S.; Liu, G. Block Copolymer Nanotubes. *Angew. Chem. Int. Ed.* **2000**, *112*, 348–352.
14. Lara, C.; Handschin, S.; Mezzenga, R. Towards Lysozyme Nanotube and 3D Hybrid Self-Assembly. *Nanoscale* **2013**, *5*, 7197–7201.
15. Shimizu, T.; Masuda, M.; Minamikawa, H. Supramolecular Nanotube Architectures Based on Amphiphilic Molecules. *Chem. Rev.* **2005**, *105*, 1401–1443.
16. Raez, J.; Manners, I.; Winnik, M. A. Nanotubes from The Self-Assembly of Asymmetric Crystalline-Coil Poly(Ferrocenylsilane-Siloxane) Block Copolymers. *J. Am. Chem. Soc.* **2002**, *124*, 10381–10395.
17. Hamley, I. W. Nanoshells and Nanotubes from Block Copolymers. *Soft Matter* **2005**, *1*, 36–43.
18. Kralj-Iglic, V.; Iglic, A.; Gomiscek, G.; Sevsek, F.; Arrigler, V.; Hagerstrand, H. Microtubes and Nanotubes of A Phospholipid Bilayer Membrane. *J. Phys. A: Math. Gen.* **2002**, *35*, 1533–1549.
19. Spector, M. S.; Singh, A.; Messersmith, P. B.; Schnur, J. M. Chiral Self-Assembly of Nanotubules and Ribbons from Phospholipid Mixtures. *Nano Lett.* **2001**, *1*, 375–378.
20. Thomas, B. N.; Safinya, C. R.; Plano, R. J.; Clark, N. A. Lipid Tubule Self-Assembly - Length Dependence on Cooling Rate Through A First-Order Phase-Transition. *Science* **1995**, *267*, 1635–1638.
21. Yager, P.; Schoen, P. E. Formation of Tubules by a Polymerizable Surfactant. *Mol. Cryst. Liq. Cryst.* **1984**, *106*, 371–381.
22. Terech, P.; de Geyer, A.; Struth, B.; Talmon, Y. Self-Assembled Monodisperse Steroid Nanotubes in Water. *Adv. Mater.* **2002**, *14*, 495–498.
23. Lu, K.; Jacob, J.; Thiyagarajan, P.; Conticello, V. P.; Lynn, D. G. Exploiting Amyloid Fibril Lamination for Nanotube Self-Assembly. *J. Am. Chem. Soc.* **2003**, *125*, 6391–6393.
24. Childers, W. S.; Mehta, A. K.; Ni, R.; Taylor, J. V.; Lynn, D. G. Peptides Organized as Bilayer Membranes. *Angew. Chem. Int. Ed.* **2010**, *49*, 4104–4107.

25. Hartgerink, J. D.; Granja, J. R.; Milligan, R. A.; Ghadiri, M. R. Self-Assembling Peptide Nanotubes. *J. Am. Chem. Soc.* **1996**, *118*, 43–50.
26. Adamcik, J.; Castelletto, V.; Bolisetty, S.; Hamley, I. W.; Mezzenga, R. Direct Observation of Time-Resolved Polymorphic States in the Self-Assembly of End-Capped Heptapeptides. *Angew. Chem. Int. Ed.* **2011**, *50*, 5495–5498.
27. Middleton, D. A.; Madine, J.; Castelletto, V.; Hamley, I. W. Insights into the Molecular Architecture of a Peptide Nanotube Using FTIR and Solid-State NMR Spectroscopic Measurements on an Aligned Sample. *Angew. Chem. Int. Ed.* **2013**, *52*, 10537–10540.
28. Ziserman, L.; Lee, H. Y.; Raghavan, S. R.; Mor, A.; Danino, D. Unraveling the Mechanism of Nanotube Formation by Chiral Self-Assembly of Amphiphiles. *J. Am. Chem. Soc.* **2011**, *133*, 2511–2517.
29. Huang, Z.; Kang, S. K.; Banno, M.; Yamaguchi, T.; Lee, D.; Seok, C.; Yashima, E.; Lee, M. Pulsating Tubules from Noncovalent Macrocycles. *Science* **2012**, *337*, 1521–1526.
30. Ghadiri, M. R.; Granja, J. R.; Milligan, R. A.; McRee, D. E.; Khazanovich, N. Self-Assembling Organic Nanotubes Based on a Cyclic Peptide Architecture. *Nature* **1993**, *366*, 324–327.
31. Zhao, F.; Ma, M. L.; Xu, B. Molecular Hydrogels of Therapeutic Agents. *Chem. Soc. Rev.* **2009**, *38*, 883–891.
32. Cheetham, A. G.; Ou, Y. C.; Zhang, P. C.; Cui, H. G. Linker-Determined Drug Release Mechanism of Free Camptothecin from Self-Assembling Drug Amphiphiles. *Chem. Commun.* **2014**, *50*, 6039–6042.
33. Cheetham, A. G.; Zhang, P. C.; Lin, L. Y.; Lin, R.; Cui, H. Synthesis and Self-Assembly of A Mikto-Arm Star Dual Drug Amphiphile Containing Both Paclitaxel and Camptothecin. *J. Mater. Chem. B* **2014**, *2*, 7316–7326.
34. Cheetham, A. G.; Zhang, P. C.; Lin, Y.-A.; Lock, L. L.; Cui, H. G. Supramolecular Nanostructures Formed by Anticancer Drug Assembly. *J. Am. Chem. Soc.* **2013**, *135*, 2907–2910.
35. Lin, R.; Cheetham, A. G.; Zhang, P. C.; Lin, Y. A.; Cui, H. G. Supramolecular filaments containing a fixed 41% paclitaxel loading. *Chem. Commun.* **2013**, *49*, 4968–4970.
36. MacKay, J. A.; Chen, M. N.; McDaniel, J. R.; Liu, W. G.; Simnick, A. J.; Chilkoti, A. Self-Assembling Chimeric Polypeptide-Doxorubicin Conjugate Nanoparticles That Abolish Tumours after A Single Injection. *Nat. Mater.* **2009**, *8*, 993–999.
37. Li, X. Y.; Yang, C. B.; Zhang, Z. L.; Wu, Z. D.; Deng, Y.; Liang, G. L.; Yang, Z. M.; Chen, H. Folic Acid as A Versatile Motif to Construct Molecular Hydrogelators through Conjugations with Hydrophobic Therapeutic Agents. *J. Mater. Chem.* **2012**, *22*, 21838–21840.
38. Duncan, R. Polymer Conjugates as Anticancer Nanomedicines. *Nat. Rev. Cancer* **2006**, *6*, 688–701.
39. Branco, M. C.; Schneider, J. P. Self-Assembling Materials for Therapeutic Delivery. *Acta Biomater.* **2009**, *5*, 817–831.
40. Aida, T.; Meijer, E. W.; Stupp, S. I. Functional Supramolecular Polymers. *Science* **2012**, *335*, 813–817.
41. Tu, R. S.; Tirrell, M. Bottom-up Design of Biomimetic Assemblies. *Adv. Drug. Deliver. Rev.* **2004**, *56*, 1537–1563.
42. Zhang, Y.; Kuang, Y.; Gao, Y. A.; Xu, B. Versatile Small-Molecule Motifs for Self-Assembly in Water and the Formation of Biofunctional Supramolecular Hydrogels. *Langmuir* **2011**, *27*, 529–537.
43. Ulijn, R. V.; Smith, A. M. Designing Peptide Based Nanomaterials. *Chem. Soc. Rev.* **2008**, *37*, 664–675.
44. Toft, D. J.; Moyer, T. J.; Standley, S. M.; Ruff, Y.; Ugolkov, A.; Stupp, S. I.; Cryns, V. L. Coassembled Cytotoxic and Pegylated Peptide Amphiphiles Form Filamentous Nanostructures with Potent Antitumor Activity in Models of Breast Cancer. *ACS Nano* **2012**, *6*, 7956–7965.
45. Behanna, H. A.; Donners, J. J. J. M.; Gordon, A. C.; Stupp, S. I. Coassembly of Amphiphiles with Opposite Peptide Polarities into Nanofibers. *J. Am. Chem. Soc.* **2005**, *127*, 1193–1200.
46. Mata, A.; Geng, Y.; Henrikson, K. J.; Aparicio, C.; Stock, S. R.; Satcher, R. L.; Stupp, S. I. Bone Regeneration Mediated by Biomimetic Mineralization of A Nanofiber Matrix. *Biomaterials* **2010**, *31*, 6004–6012.
47. Hamley, I. W.; Dehsorkhi, A.; Castelletto, V. Coassembly in Binary Mixtures of Peptide Amphiphiles Containing Oppositely Charged Residues. *Langmuir* **2013**, *29*, 5050–5059.
48. Kaler, E. W.; Herrington, K. L.; Murthy, A. K.; Zasadzinski, J. A. N. Phase-Behavior and Structures of Mixtures of Anionic and Cationic Surfactants. *J. Phys. Chem.* **1992**, *96*, 6698–6707.
49. Marques, E. F.; Regev, O.; Khan, A.; Miguel, M. D.; Lindman, B. Vesicle Formation and General Phase Behavior in the Catanionic Mixture SDS-DDAB-Water. The Anionic-Rich Side. *Phys. Chem. B* **1998**, *102*, 6746–6758.
50. Tondre, C.; Caillet, C. Properties of the Amphiphilic Films in Mixed Cationic/Anionic Vesicles: A Comprehensive View from A Literature Analysis. *Adv. Colloid Interface Sci.* **2001**, *93*, 115–134.
51. Leung, C. Y.; Palmer, L. C.; Qiao, B. F.; Kewalramani, S.; Sknepnek, R.; Newcomb, C. J.; Greenfield, M. A.; Vernizzi, G.; Stupp, S. I.; Bedzyk, M. J.; de la Cruz, M. O. Molecular Crystallization Controlled by pH Regulates Mesoscopic Membrane Morphology. *ACS Nano* **2012**, *6*, 10901–10909.
52. Dubois, M.; Deme, B.; Gulik-Krzywicki, T.; Dedieu, J. C.; Vautrin, C.; Desert, S.; Perez, E.; Zemb, T. Self-Assembly of Regular Hollow Icosahedra in Salt-Free Catanionic Solutions. *Nature* **2001**, *411*, 672–675.
53. Zemb, T.; Dubois, M.; Deme, B.; Gulik-Krzywicki, T. Self-Assembly of Flat Nanodiscs in Salt-Free Catanionic Surfactant Solutions. *Science* **1999**, *283*, 816–819.
54. Manghisi, N.; Leggio, C.; Jover, A.; Meijide, F.; Pavel, N. V.; Tellini, V. H. S.; Tato, J. V.; Agostino, R. G.; Galantini, L. Catanionic Tubules with Tunable Charge. *Angew. Chem. Int. Ed.* **2010**, *49*, 6604–6607.
55. Nelson, R.; Sawaya, M. R.; Balbirnie, M.; Madsen, A. O.; Riekel, C.; Grothe, R.; Eisenberg, D. Structure of the Cross-[Beta] Spine of Amyloid-Like Fibrils. *Nature* **2005**, *435*, 773–778.
56. Cui, H.; Hodgdon, T. K.; Kaler, E. W.; Abezgauz, L.; Danino, D.; Lubovsky, M.; Talmon, Y.; Pochan, D. J. Elucidating the Assembled Structure of Amphiphiles in Solution *via* Cryogenic Transmission Electron Microscopy. *Soft Matter* **2007**, *3*, 945–955.
57. Helfrich, W.; Prost, J. Intrinsic Bending Force In Anisotropic Membranes Made of Chiral Molecules. *Phys. Rev. A* **1988**, *38*, 3065–3068.
58. Selinger, J. V.; Spector, M. S.; Schnur, J. M. Theory of Self-Assembled Tubules and Helical Ribbons. *J. Phys. Chem. B* **2001**, *105*, 7157–7169.
59. Israelachvili, J. N. *Intermolecular and Surface Forces*, 3rd ed.; Elsevier: New York, 2011.
60. Adamcik, J.; Mezzenga, R. Adjustable Twisting Periodic Pitch of Amyloid Fibrils. *Soft Matter* **2011**, *7*, 5437–5443.
61. Adamcik, J.; Mezzenga, R. Proteins Fibrils from a Polymer Physics Perspective. *Macromolecules* **2012**, *45*, 1137–1150.
62. Usov, I.; Adamcik, J.; Mezzenga, R. Polymorphism Complexity and Handedness Inversion in Serum Albumin Amyloid Fibrils. *ACS Nano* **2013**, *7*, 10465–10474.
63. Adamcik, J.; Lara, C.; Usov, I.; Jeong, J. S.; Ruggeri, F. S.; Dietler, G.; Lashuel, H. A.; Hamley, I. W.; Mezzenga, R. Measurement of Intrinsic Properties of Amyloid Fibrils by the Peak Force QNM Method. *Nanoscale* **2012**, *4*, 4426–4429.
64. Usov, I.; Mezzenga, R. Correlation between Nanomechanics and Polymorphic Conformations in Amyloid Fibrils. *ACS Nano* **2014**, *8*, 11035–11041.
65. Geng, Y.; Dalhaimer, P.; Cai, S. S.; Tsai, R.; Tewari, M.; Minko, T.; Discher, D. E. Shape Effects of Filaments *versus* Spherical Particles in Flow and Drug Delivery. *Nat. Nanotechnol.* **2007**, *2*, 249–255.
66. Jiang, S. Y.; Cao, Z. Q. Ultralow-Fouling, Functionalizable, and Hydrolyzable Zwitterionic Materials and Their Derivatives for Biological Applications. *Adv. Mater.* **2010**, *22*, 920–932.

67. Dubikovskaya, E. A.; Thorne, S. H.; Pillow, T. H.; Contag, C. H.; Wender, P. A. Overcoming multidrug resistance of small-molecule therapeutics through conjugation with releasable octaarginine transporters. *Proc. Natl. Acad. Sci. U.S.A.* **2008**, *105*, 12128–12133.